Supplementary Tables

Suppl. Table 1: Data collection and refinement statistics

	Free canakinumab Fab	Canakinumab complex with IL-1β
Data collection		
X-ray source	SLS beamline XS06A	FR-E rotating anode
Wavelength	0.97950Å	1.54178Å
Detector type	MAR165 CCD	MAR345 DTB Imaging plate
Number of crystals	1	1
Space group	$P2_1$	$P2_12_12_1$
Cell dimensions		
a, *b*, *c* (Å)	80.62, 142.26, 83.80	50.93, 56.28, 191.70
α, β, γ (°)	90.00, 115.76, 90.00	90.00, 90.00, 90.00
Resolution (Å)	2.00 (2.07-2.00)	2.20 (2.28-2.20)
Number of molecules in asymmetric unit	4 Fabs	1 Fab complex
R_{sym} or R_{merge}	0.057 (0.148)	0.038 (0.179)
$I / \sigma(I)$	11.7 (4.4)	24.7 (7.3)
Completeness (%)	100.0 (99.9)	99.0 (99.8)
Redundancy	4.8 (4.5)	7.0 (6.7)
Refinement		
Resolution (Å)	50.81-2.00	49.22-2.20
No. reflections/test reflections	114,268	28,599/1,459
R_{work} / R_{free}	0.186/0.228	0.188/0.231
No. atoms		
Protein	13,207	4,489
Buffer ions	-	2 x Cl^-
Water	1,234	254
B-factors (Å^2)		
Protein	24.3	55.0
Buffer ions	-	59.2
Water	32.2	45.8
R.m.s. deviations		
Bond lengths (Å)	0.006	0.010
Bond angles (°)	1.4	1.18
Ramachandran outliers	Ala51 (chain A, C, E, G)	Ala51 (chain L)

(Values in parentheses are for the highest resolution shell)

Supplementary Figures

Suppl. Figure 1: Final (2Fo-Fc) electron-density maps

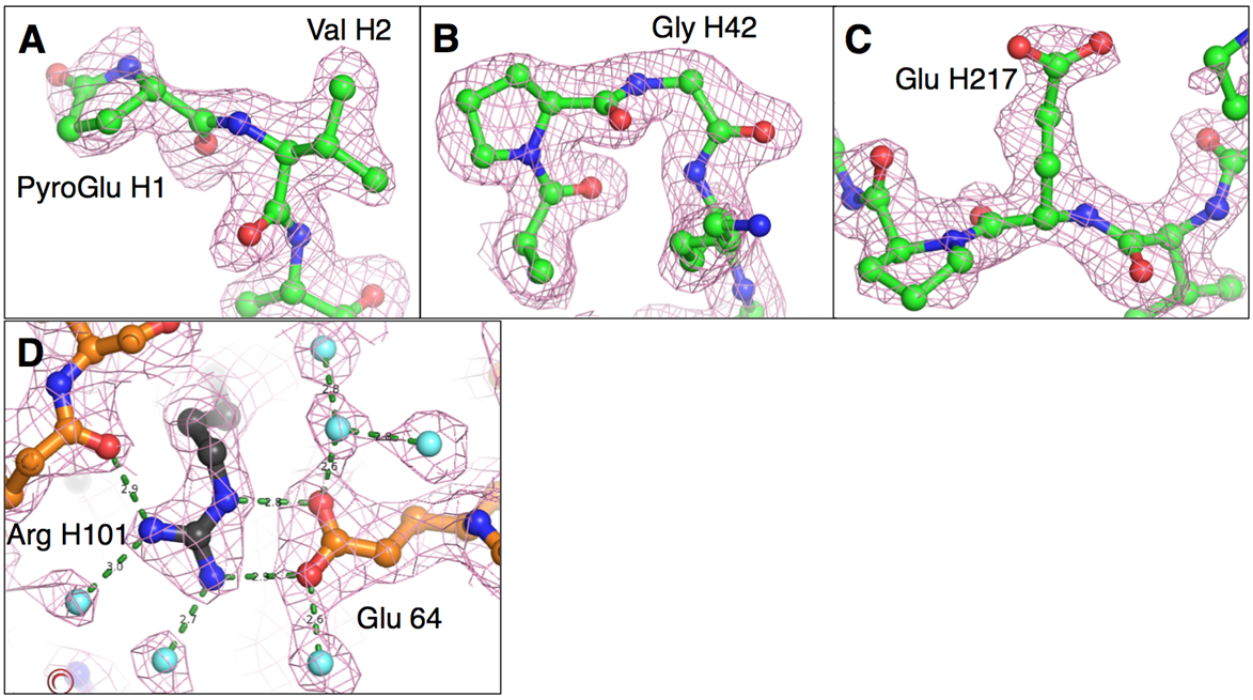

Suppl. Figure 1: The final (2Fo-Fc) electron-density is shown (1.0σ contour) for selected regions, differing from the previously reported structures.[14] **A**, **B** and **C**: free canakinumab Fab. **A.** N-terminus of the heavy-chain: the electron-density is consistent with the presence of a pyroglutamic acid residue. **B.** Residues 41-43 of the heavy-chain: the electron-density is consistent with the presence of a glycine at position 42. **C.** Residues 216-218 of the heavy-chain: the electron-density is consistent with the presence of a glutamate at position 217. **D**: IL-1β complex. Interaction between Glu 64 of IL-1β and Arg H101 of canakinumab. Note the short contact between Glu 64 Oε2 and Arg H101 Nε.

Suppl. Figure 2: Crystal structure of the free canakinumab Fab. Conformation of H-CDR3

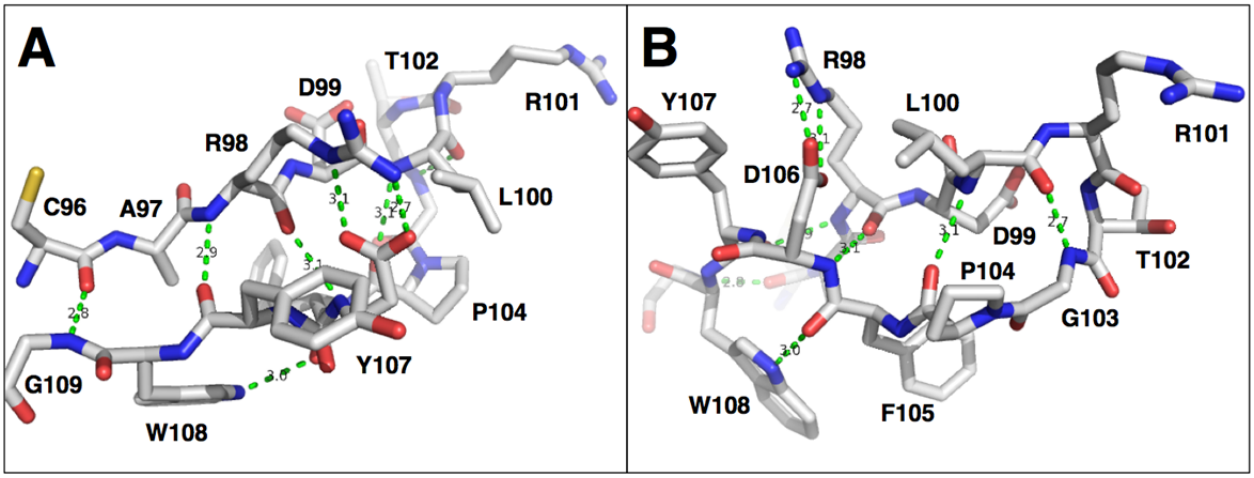

Suppl. Figure 2: The conformation of H-CDR3 of canakinumab in the free state. **A.** Buldged *torso* region of H-CDR3, exhibiting the typical salt-bridge interaction between Asp H106 and Arg H98, and the H-bonded contact between the main-chain carbonyl oxygen of Asp H106 and the side-chain of Trp H108. **B.** Head region of H-CDR3 with a *trans*-proline at position H104.

Suppl. Figure 3 : Topology of the canakinumab epitope on human IL-1β

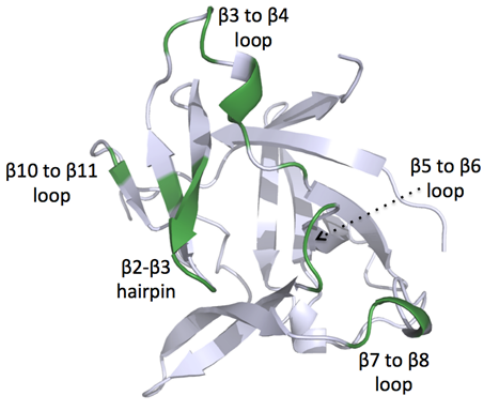

Suppl. Figure 3: Human IL-1β is shown in cartoon representation with the structural elements constituting the canakinumab epitope highlighted in deep green.

Suppl. Figure 4: The canakinumab paratope

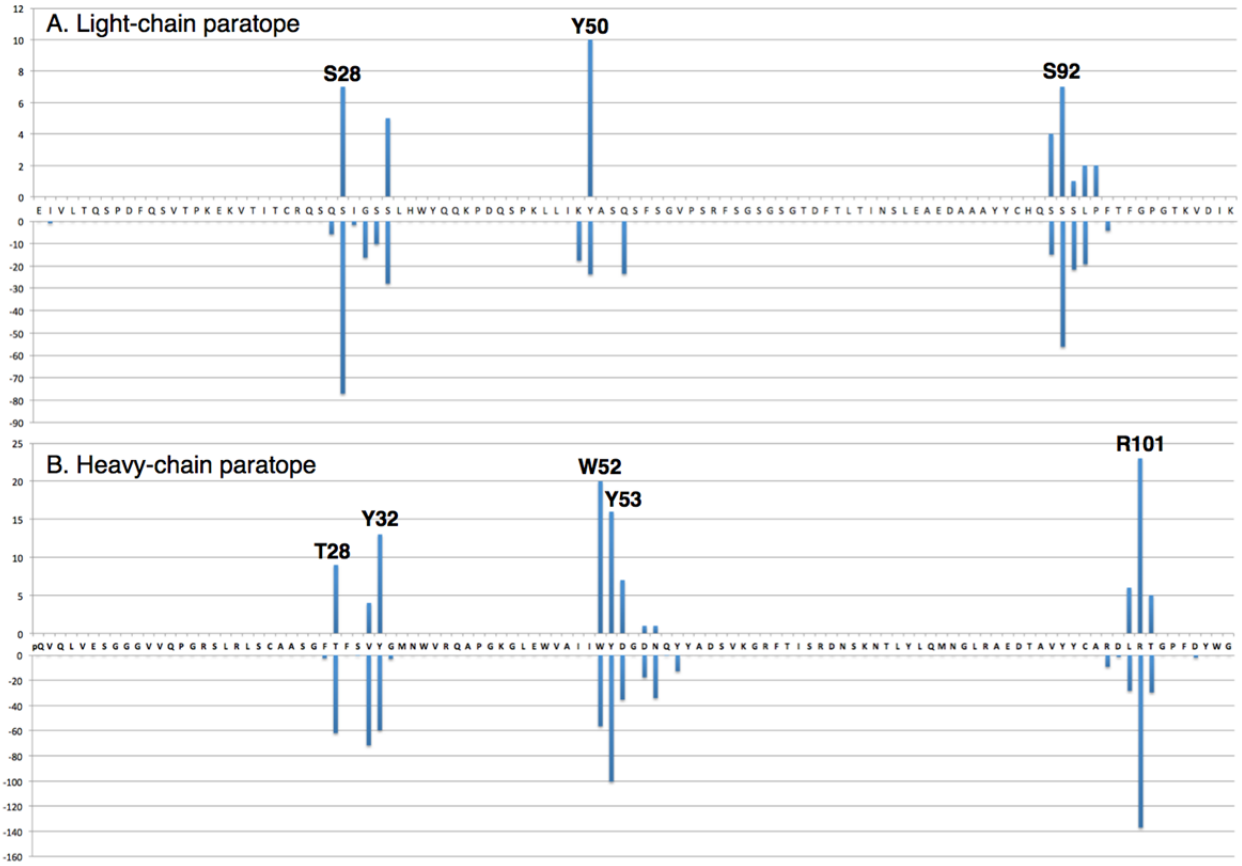

Suppl. Figure 4: The canakinumab paratope. **A.** The amino-acid sequence of the variable domain of the canakinumab light-chain is shown on the horizontal axis together with the number of direct intermolecular contacts to IL-1β (3.9Å distance cut-off; Y-axis, upper half) and the reduction in solvent-accessible surface upon antigen binding (in $Å^2$; Y-axis, lower half). **B.** Same as above for the heavy-chain of canakinumab. Note the involvement of all six CDRs in antigen binding, including in particular L-CDR2.

Suppl. Figure 5: The canakinumab epitope on human IL-1β

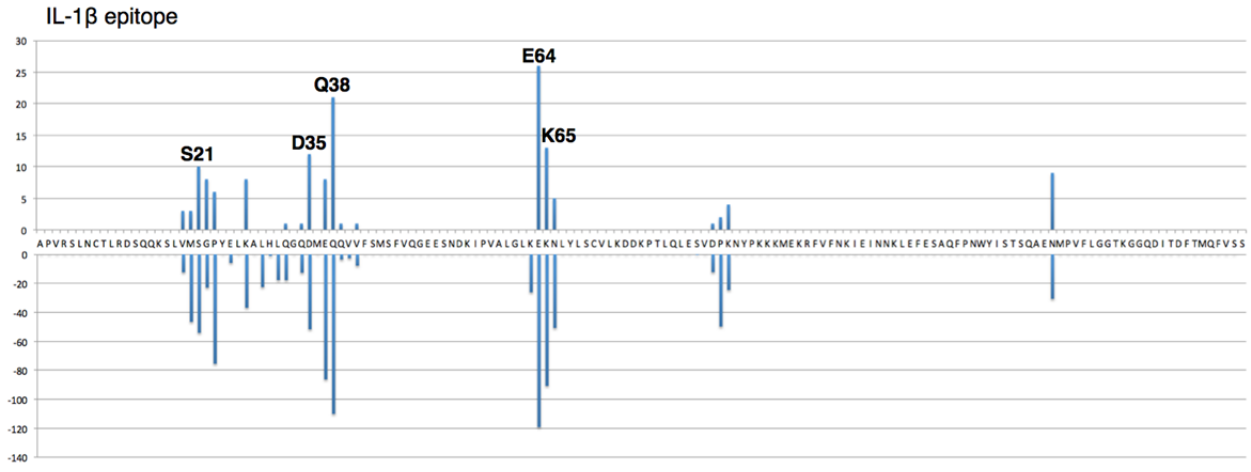

Suppl. Figure 5: The canakinumab epitope on human IL-1β. **A.** The amino-acid sequence of human IL-1β is shown on the horizontal axis together with the number of direct intermolecular contacts to IL-1β (3.9Å distance cut-off; Y-axis, upper half) and the reduction in solvent-accessible surface upon antibody binding (in $Å^2$; Y-axis, lower half).

Suppl. Figure 6: Close-up views of binding interactions between canakinumab and IL-1β

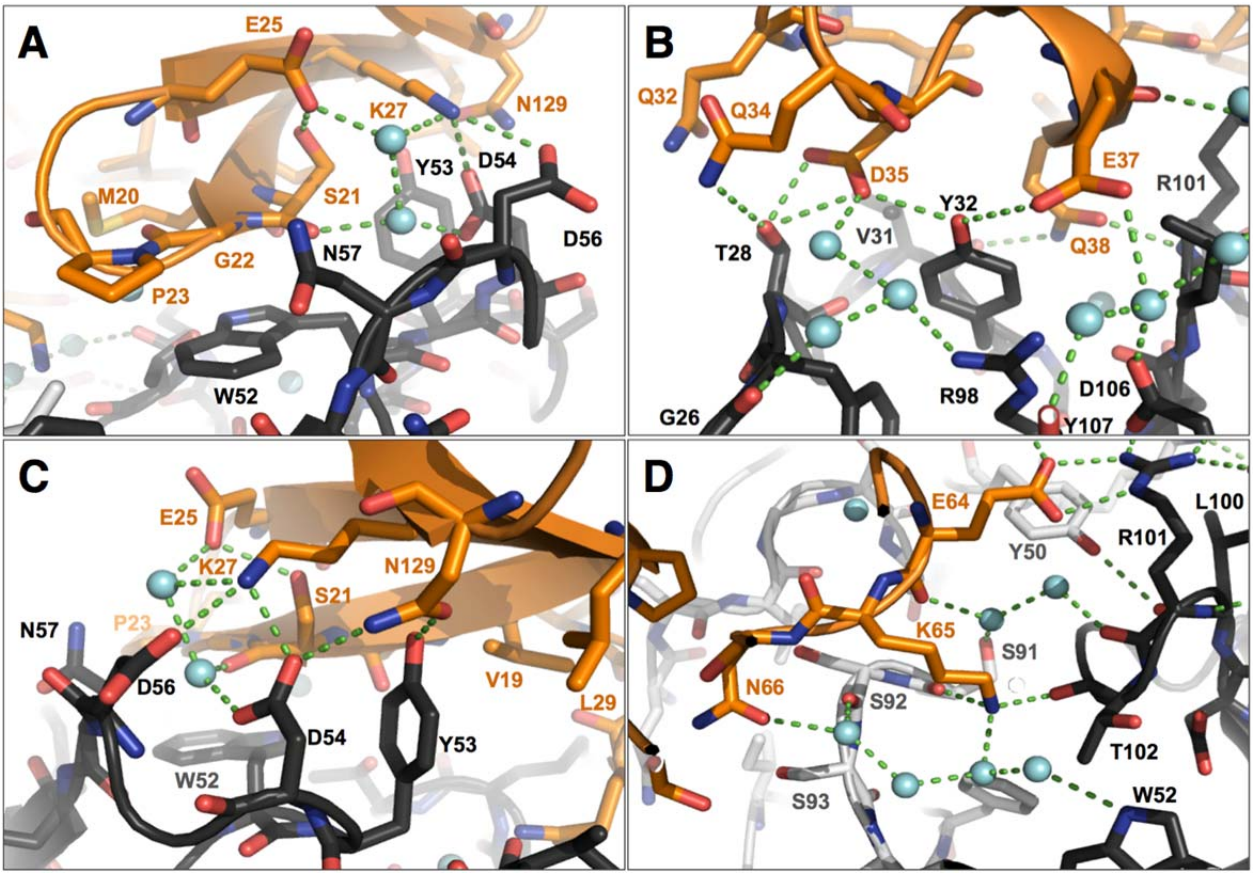

Suppl. Figure 6: Close-up view of binding interactions between canakinumab and human IL-1β. Heavy- and light-chain paratope residues are in black and light-grey sticks, respectively, while epitope residues are in orange. Light-blue spheres denote water molecules, dashed lines close contacts (< 3.5Å). **A.** Binding interactions involving the β2-β3 β-hairpin of IL-1β. Note the hydrophobic contacts of Gly 22 and Pro 23 with the Trp H52 side-chain and the electrostatic interactions of Lys 27 with Asp H54 and Asp H56. **B.** Binding interactions involving the β3 to β4 loop of IL-1β. Note the H-bonded contacts made by Gln 34, Asp 35, Glu 37 and Gln 38. **C.** Binding interactions involving the β10 to β11 loop of IL-1β. Note the H-bonded contacts made by Asn 129. **D.** Binding interactions involving the β5 to β6 loop of IL-1β.

Note in particular the H-bonded contacts made by Lys 65, the salt-bridge interaction between Glu 64 and Arg H101 and the anion-π interaction of Glu 64 with Tyr L50.

Suppl. Figure 7: Conformational change affecting the β5 to β6 loop of IL-1β

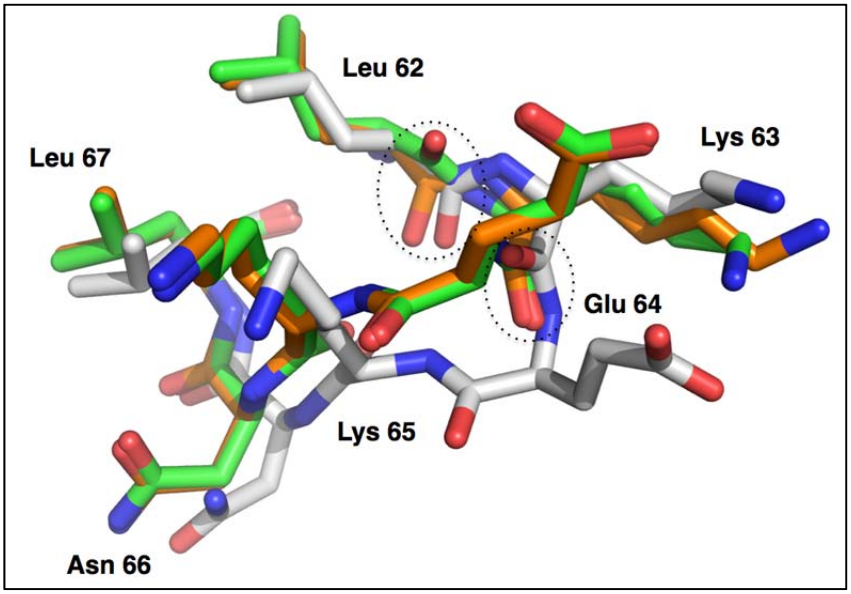

Suppl. Figure 7: Conformational change affecting the β5 to β6 loop of IL-1β. Structural overlay showing the β5 to β6 loop of IL-1β (amino-acid residues 62 to 67) in the free state (PDB entry 2I1B, grey stick) and in the canakinumab-bound state (orange stick, this work; green stick, PDB entry 4G6J). Note the large shift of Glu 64 and the flip of the Lys 63 – Glu 64 peptide bond (dashed circle). Note that the orientation of the Leu 62 – Lys 63 peptide bond of the antibody-bound state is similar to that of the free state in the work reported here.

Suppl. Figure 8: Amino acid comparison between human and non-human primate mature IL-1β

```
                    1                                                    60
Human IL-1β         APVRSLNCTLRDSQQKSLVMSGPYELKALHLQGQDMEQQVVFSMSFVQGEESNDKIPVAL
Marmoset IL-1β      APVRSLNCTLRDAQQKCLVMSGPYELKALHLQGQDLEQQVVFSMSFVQGEESNDKIPVAL
Cyno IL-1β          APVRSLHCTLRDAQLKSLVMSGPYELKALHLQGQDLEQQVVFSMSFVQGEESNDKIPVAL
                    ****** *****:* *.******************:**********************
                    61                                                   120
Human IL-1β         GLKEKNLYLSCVLKDDKPTLQLESVDPKNYPKKKMEKRFVFNKIEINNKLEFESAQFPNW
Marmoset IL-1β      GLKEKNLYLSCVLKDKKPTLQLESVDPKNYPKKKMEKRFVFNKTEINNKLEFESAQFPNW
Cyno IL-1β          GLKAKNLYLSCVLKDDKPTLQLESVDPKNYPKKKMEKRFVFNKIEINNKLEFESAQFPNW
                    *** **********.************************** ***************
                    121
Human IL-1β         YISTSQAENMPVFLGGTKGGQDITDFTMQFVSS
Marmoset IL-1β      YISTSQAENMPVFLGGTKGGQDITDFTMQFVS-
Cyno IL-1β          YISTSQAENMPVFLGGTRGGQDITDFTMQFVS-
                    *****************:**************
```

Suppl. Figure 9: Mechanism of IL-1β neutralization by canakinumab

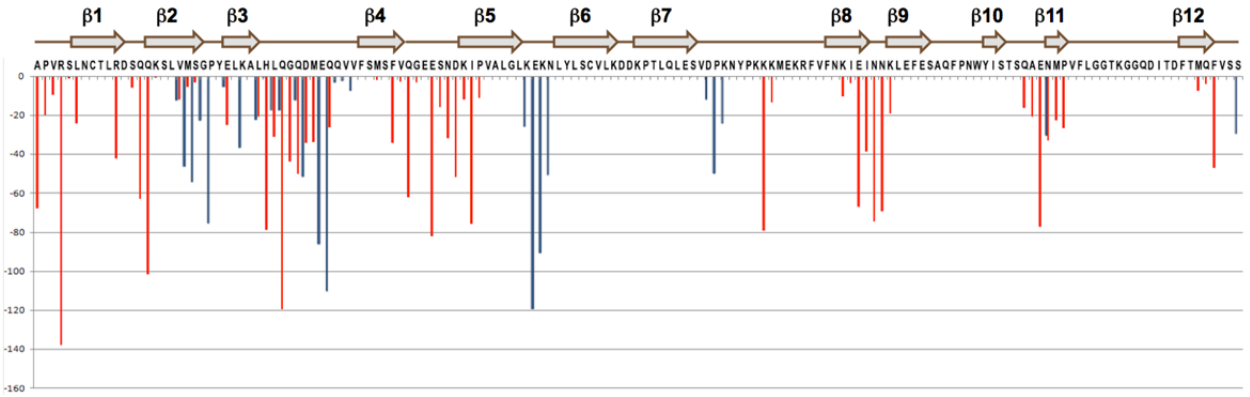

Suppl. Figure 9: Graph showing the reduction (Y axis, in $Å^2$) in solvent-accessible surface of IL-1β residues (X axis) upon binding to IL-1RI (red bars) or canakinumab (blue bars). The amino-acid sequence of IL-1β is shown together with the corresponding secondary structure elements. Note the overlap

between the two binding interfaces, notably in the region of the amino-acids Val 19 to Glu 25 and Leu 29 to Gln 38.